A simple feature extraction method for estimating the whole life cycle state of health of lithium-ion batteries using transformer-based neural network

A simple feature extraction method for estimating the whole life cycle state of health of lithium-ion batteries using transformer-based neural network

Kai Luo[a], Huiru Zheng[b], Zhicong Shi[a,*]

[a] *School of Materials and Energy, Guangdong University of Technology, Guangzhou 510006, Guangdong, China*
[b] *School of Computing, Ulster University, Belfast, BT15 1ED, United Kingdom*

[*]Corresponding authors.
E-mail addresses: zhicong@gdut.edu.cn (Z.C. Shi)

Abstract

Accurately estimating the state of health (SOH) of lithium-ion batteries (LIBs) can avoid safety accidents and economic losses, and it remains a big research challenge. In this paper, electrochemical impedance spectroscopy (EIS) is used as the feature for the SOH prediction. EIS contains rich information such as material properties and electrochemical reactions, which directly reflects the aging state of LIBs. In order to obtain valuable data for SOH estimation, we propose a new feature extraction method from the perspective of electrochemistry, and then apply the transformer-based neural network for SOH estimation. Through feature extraction, the mean absolute percentage error of the estimation is reduced to 1.63% in the whole life cycle, which is decreased by 70% compared to the original data before feature extraction.

Keywords: lithium-ion battery; state of health; electrochemical impedance spectroscopy; transformer neural network; data-driven

1 Introduction

Limited fossil fuel reserves and climate change challenges have greatly promoted the application of lithium-ion batteries (LIBs) in all walks of life. However, with the continuous occurrence of accidents, more attention has been paid to safety issues.[1] As time goes on, LIBs will gradually degenerate and capacity will continue to decline.[2] State of health (SOH) is usually defined as the current capacity as a percentage of the nominal capacity,[3] as shown in equation (1). Accurate prediction of SOH is crucial to ensure the economic value of equipment and its safety.

$$SOH = \frac{C_{\text{full}}}{C_{\text{norm}}} \times 100\% \quad (1)$$

Where C_{full} and C_{norm} represent the capacity of the fully charged state and the nominal capacity respectively.

Traditional model-based methods include the electrochemical model and equivalent circuit model (ECM).[4] The electrochemical model is based on the reaction kinetics and porous electrode theory. In order to better describe the formation of the solid electrolyte interface (SEI) layer at the molecular level, Methekar et al. [5] used dynamic Monte Carlo simulation to solve the problem of surface heterogeneity, which promotes the further development of the formation mechanism of SEI film. The ECM is created based on a combination of circuit elements that produce the same electrical behavior as the cell.[6] Based on the internal resistance growth model, several different particle filters were proposed for improving the performance of the filtering algorithm. Establishing the mechanism model requires a deep understanding of the various reaction mechanisms inside the LIBs. Although these models were established by the

electrochemical behavior of the cell, various complicate reactions lead to high complexity.[7] ECM is easier to establish, but they are limited in estimating the long-term state since the nonlinear changes in internal parameters of the battery during operation.[8]

With the rapid development of artificial intelligence, data-driven methods become popular. [9, 10] In recent years, since deep learning does not consider the complex electrochemical reactions inside the LIBs and has shown amazing performance in various tasks, significant progress has been made in estimating LIBs degeneration.[11] Khumprom et al. [12] predicted the SOH and remaining useful life of LIBs by a deep neural network (DNN). Song et al. [13] analyzed the ageing trend based on a data platform. Roman et al. [14] proposed a machine learning pipeline that estimates LIBs SOH and algorithm uncertainty in real-time. Yang et al. [15] handled partial SOH between two consecutive charge/discharge cycles through a convolutional neural network (CNN). Shen et al. [16] predicted the capacity of the LIBs using CNN with current and voltage data.

For time-series prediction tasks, in addition to the DNN and CNN, recurrent neural network (RNN)-based models are generally better due to their memory function, which includes RNN and two variants of long short-term memory (LSTM) neural work (NN) and Gated Recurrent Unit (GRU) NN. [17, 18] Eddahech et al. [19] have proved that RNN can be used for predicting LIBs degradation. Heinrich et al. [20] used LSTM NN for SOH estimation based on the virtual execution of LIBs experiments. A large amount of heat will be released during operation, which can be extracted as health indicators for

SOH estimation.[21] Cui et al. [22] extracted features during operation and introduced dynamic spatiotemporal attention-based GRU NN for SOH estimation. However, RNN-based models have some issues, one of which is the long-term dependencies caused by gradient disappearance or gradient explosion.

Since typical battery management systems generally collect current, voltage, and temperature, extracting features from charging and discharging curves to input models is the most used method at present.[23] Compared with the usual current-voltage data, electrochemical impedance spectroscopy (EIS) measures the current (voltage) response to voltage (current) perturbation, to obtain multi-dimensional information including all material properties, interface phenomena, and electrochemical reactions inside the cell.[24] EIS tracks the state of the LIBs and is one of the direct health indicators of degeneration. However, in general, in order to include the electrochemical reactions contained in the cell, the frequency range of the EIS is wide, usually from 10^{-3} Hz to 10^{7} Hz, which means that EIS data are high-dimensional, usually with hundreds of features. A few data deserve attention because they are the core of the EIS spectrum, the changes of most data are affected by them and illustrate the changes in the battery's internal ohmic resistance, polarization resistance and Warburg resistance to predict the ageing state.

In order to address the above problems, this paper proposes a simple features extraction method for EIS, which extracts features related to SOH from the ohmic resistance, the resistance of lithium-ion passing through the SEI layer, the charge transfer resistance, and the diffusion impedance, and then uses the transformer-based NN to estimate the

SOH of LIBs. Extracting key features not only simplifies data, but also reduces the amount of computation. The attention mechanism focuses on the important features and builds long-term associations. It is a simple and efficient method.

The main contribution of this paper is to extract EIS features through electrochemical cognition to accurately estimate the SOH of LIBs. EIS data can be explained by a traceable electrochemical mechanism, and the changes directly relate to the SOH. Compared to other complex feature engineering approaches, the proposed feature screening from the perspective of electrochemistry is a simple and effective method to focus on valuable data. Moreover, due to the high dimensionality of information contained in EIS, the self-attention mechanism is adopted to make the model pay more attention to the influential features. And considering the amount of data used, the calculation module in the model is reduced to reduce the parameters. The results show that transformer-based NN performs better than the RNN-based model in obtaining information from the whole input and has superior performance in processing long-term data. The pipeline is shown in Figure 1.

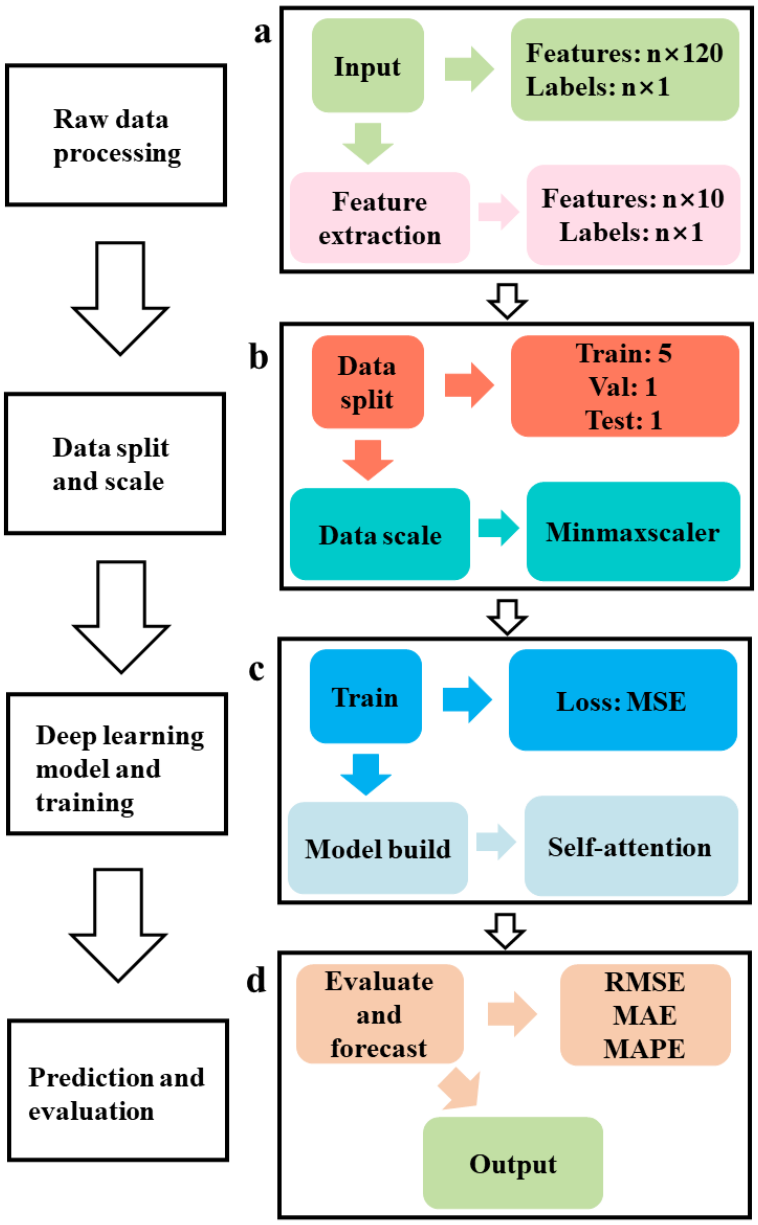

Fig. 1. Pipeline diagram of SOH estimation method. (a) Extract features from the raw data, and reduce the feature dimensions from 120 to 10. (b) The number of cells used in this study is 7, and the training set, validation set and test set are 5, 1 and 1 respectively. (c) The deep learning model is established and trained. The loss function used is MSE. (d) Evaluate through RMSE, MAPE and MAE and obtain the output

2 Methods

The transformer-based NN bases on the self-attention mechanism to deal with sequence problems. It has been successfully applied in the fields of sense interpretation,[25] image recognition,[26] and sentimental analysis,[27] as well as has shown superior performance compared with previous RNN-based models. [28, 29]

EIS of LIBs contains abundant information about the internal changes of the LIBs, which can show the differences in electrochemical behavior during aging.[30] Aiming at the high dimensionality of EIS and the long time series behavior of cycle life, the transformer-based NN presents better performances in identifying the noteworthy features.

2.1 Model Structure

Different from the traditional recurrent structure, transformer-based NN only calculates the implicit representation of model input and output through the attention mechanism. The data calculates through two attention blocks, which contain multi-head attention, residual connection, and layer normalization, then passes through two linear layers and finally gets the output.[29]

2.2 Attention mechanism

The attention mechanism can be described as the process of mapping a query and a series of key-value pairs to an output, and the output vector is the sum of the weights on the value calculated according to the query and key. The

advantage is the higher ability to find the dependency relationship between different sequence positions, which means a stronger ability to capture the interaction relationship between long-term data.[31] The calculation of attention is shown in equations (2), (3), and (4).

$$\boldsymbol{Q} = \boldsymbol{x}\boldsymbol{W}^{\mathbf{Q}} \tag{2}$$

$$\boldsymbol{K} = \boldsymbol{x}\boldsymbol{W}^{\mathbf{K}} \tag{3}$$

$$\boldsymbol{V} = \boldsymbol{x}\boldsymbol{W}^{\mathbf{V}} \tag{4}$$

where Q, K, and V are matrices of Query, Key, and Value, respectively; $W^{\mathrm{Q}} \in R^{\mathrm{M\times dq}}$, $W^{\mathrm{K}} \in R^{\mathrm{M\times dk}}$, and $W^{\mathrm{V}} \in R^{\mathrm{M\times dv}}$ are matrices that need to learn from the EIS; M, $\boldsymbol{dq}$, $\boldsymbol{dk}$ and $\boldsymbol{dv}$ are the quantity of entered vector, dimension of Q, dimension of K, and the dimension of V.

The calculation of self-attention is shown in equation (5) and Figure 2. First, Q and K are multiplied (MatMul) to obtain a score representing the dependency between different positions. Then, to get a more stable gradient, it is divided by $\sqrt{\boldsymbol{d}_{\mathbf{k}}}$ (Scale). Finally, after the softmax processing, the final value is obtained by multiplying with V (MatMul).

$$\mathbf{Attention}\,(\boldsymbol{Q},\boldsymbol{K},\boldsymbol{V}) = \mathbf{softmax}\left(\frac{\boldsymbol{Q}\boldsymbol{K}^{\mathbf{T}}}{\sqrt{\boldsymbol{d}_{\mathbf{k}}}}\right)\boldsymbol{V} \tag{5}$$

where $\boldsymbol{dk}$ is the dimension of K.

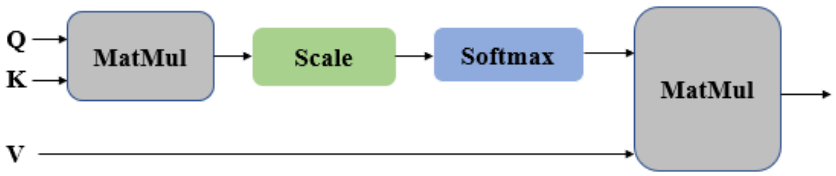

Fig. 2. Attention calculation process. After Q and K are multiplied (MatMul), scaled and softmaxed, the result is multiplied by V to obtain the output

2.3 Dataset

The EIS public dataset is used in this study. The dataset contains EIS data obtained from ten different states and the corresponding capacity, which is available from the Cavendish Laboratory of the University of Cambridge.[32] The experimental data was collected by electrochemical tests on the commercially available 45 mAh Eunicell LR2032 LIBs at 25 ℃, 35 ℃, and 45 ℃ with the charge and discharge current at 1C (45mA) and 2C (90mA) rates. The chemical composition of the cells is $LiCoO_2$ / graphite, and the upper and lower voltage limits are 4.2V and 3V respectively. The EIS data selected in this experiment are taken ten minutes after certain discharge. The difference in EIS data between different cycles of one cell is shown in Figure 3.

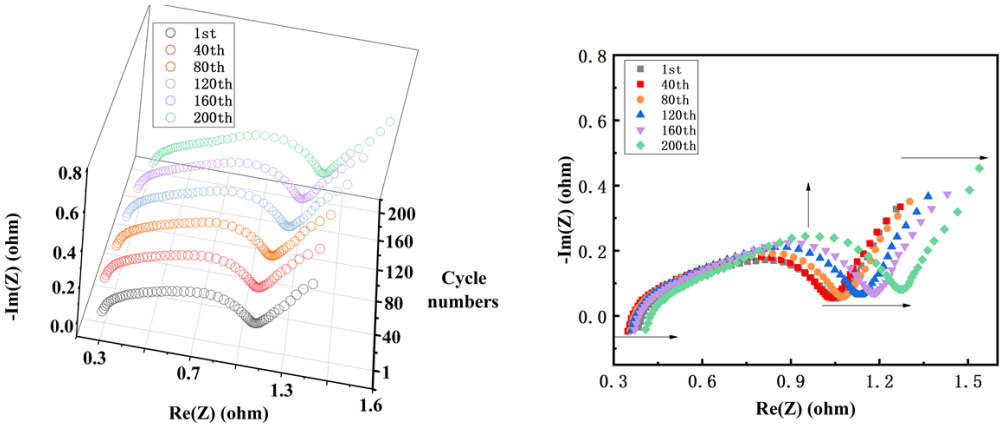

Fig. 3. EIS data between different cycles of one cell. (a) 3D schematic diagram of EIS changes in the whole life cycle of one LIB, (b) plane figure corresponding to (a). The gray circle, red circle, orange circle, blue circle, purple circle, and green circle represent the EIS after 1 cycle, 40 cycles, 80 cycles, 120 cycles, 160 cycles and 200 cycles respectively. The difference in the EIS curve shape between different cycles is shown in (b), marked with black arrows. And the significance of the EIS curve shape difference between different cycles is described later

EIS analyzes electrode process dynamics, electric double layer, and diffusion, which directly reflect the degradation of LIBs' physical performance. Generally, the EIS obtained in a frequency range of 10^{-3} Hz to 10^{7} Hz is composed of dozens and hundreds of points. These data can provide abundant internal change information about the LIBs, but only a few points are highly relevant, and more input features make the correlation more challenging to detect, resulting in the risk of reducing the prediction accuracy. Therefore, through feature extraction, the impedance reflecting the high correlation between the loss of conductivity, lithium ions and the active substance is screened to relate the SOH of the LIB. Therefore, we propose a new method to extract the features of EIS data from the perspective of electrochemistry.

2.4 Feature selection

The proposed feature extracting method is shown in Figure 4. Features are directly extracted from the original data. The original data has 60 feature points (120 dimensions), and the final extracted feature is 5 points (10 dimensions), which has the highest correlation with SOH. On the premise of retaining the key data, four successive feature extraction is carried out, and almost half of the data is removed each time to prove the effectiveness of the proposed method.

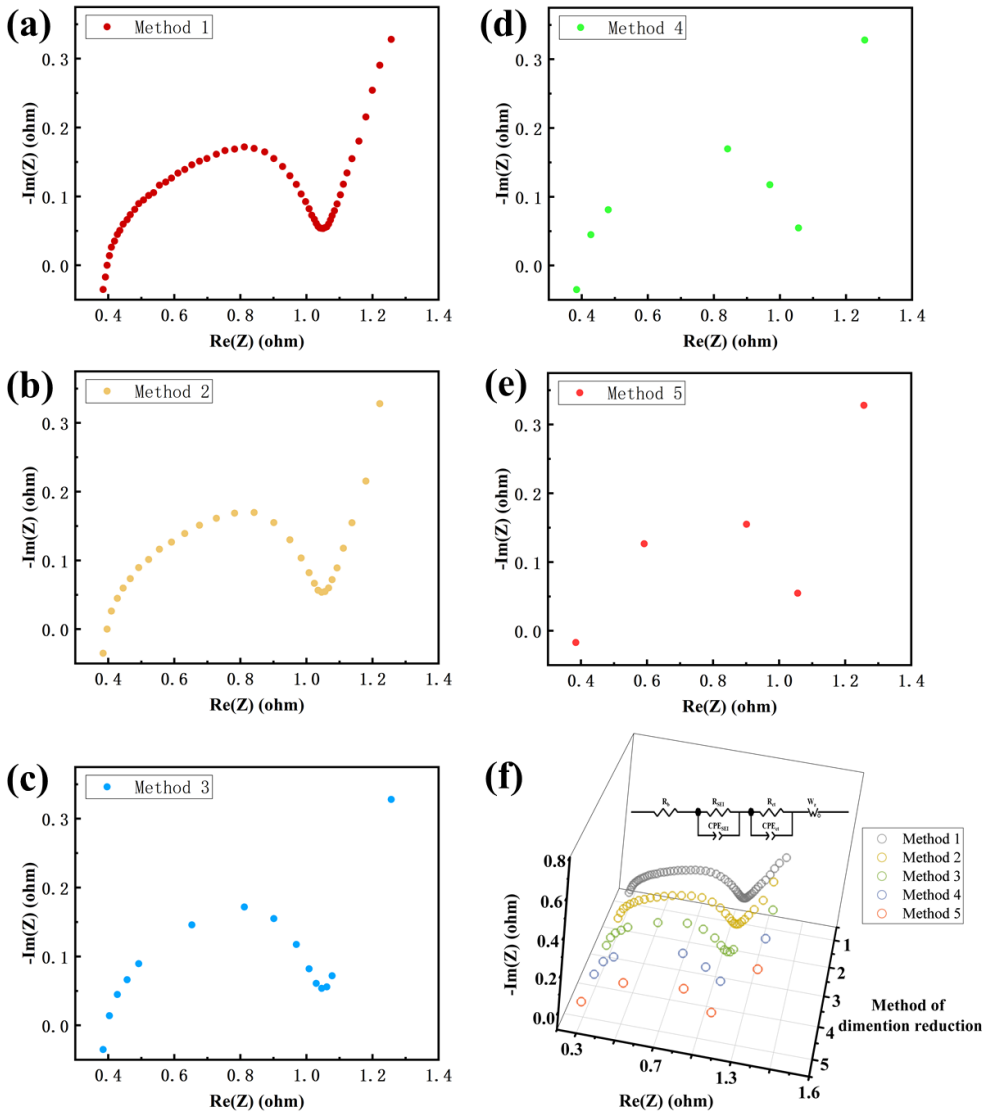

Fig. 4. Schematic diagram of the feature extraction process. (a) Method1, which means the original data. (b) Method2, which means extracting 50% from the original data. (c) Method3, which means extracting 25% from the original data. (d) Method4, which means extracting 12% from the original data. (e) Method5, which means extracting 8% from the original data. (f) Schematic diagram of the equivalent circuit and feature extraction from original data for one EIS curve

The EIS spectrum demonstrates the characteristics of electron transfer, ions diffusion in the electrolyte, SEI layer and solid active material, as well as charge transfer in the

electric double layer.[33] Two intersecting semicircles and one sloping line plot and the equivalent circuit corresponding to EIS are shown in Figure 4 (f). The EIS spectrum of LIBs normally includes overlapped semicircles and a diagonal line, indicating the electron transportation, the charge transfer, and the ion diffusion process, respectively. Therefore, the equivalent circuit is a circuit in which one resistor is connected in series with two resistors and capacitors in parallel, and finally a Warburg impedance is connected in series. As the intersection of the high-frequency region on X axis, R_o represents internal ohmic resistances for the transport of electrons through the collector and active material particles, as well as lithium ions through the electrolyte. The semicircle in the high-frequency region is attributed to a surface process, R_{sei} and CPE_{SEI} mean the diffusion and migration of lithium ions through the insulating layer on the surface of active material particles. The semicircle in the middle-frequency region represents R_{ct} and CPE_{ct}, which are related to the charge transfer in the electric double layer. And the sloping line in the low-frequency region represents Z_w, which signifies the solid diffusion process of lithium ions in active material particles.

The degradation can be reflected by the loss of conductivity, lithium ions, and active materials. R_o is attributed to the resistance caused by the contact loss between collector and binder, as well as electrode particles and electrolyte, and the increase is related to the loss of conductivity, represented by the intersection on X axis in the EIS spectrum in the high-frequency region. The formation of the SEI layer hinders the transfer of lithium ions between electrodes and reduces the number of lithium ions embedded / removed during charging / discharging. The irreversible loss of lithium ions reduces the

concentration of lithium ions, making the charge transfer process more difficult. The loss of lithium ions leads to the enlargement of the semicircle in the high-frequency region and middle-frequency region, represented by the intersection of the first semicircle and the second semicircle and the endpoint of the second semicircle. The Warburg resistance linear part represents diffusion in the EIS spectrum. The structural collapse of active materials leads to the difficulty of lithium ions diffusion in electrode solid particles due to the lengthening of the sloping line caused by the loss of active materials, represented by the last point of the Warburg resistance linear part representing diffusion in the EIS spectrum. The above behaviors will lead to a reduction in the available capacity of LIB.

In this study, the semicircle representing the high frequency coincides with the semicircle representing the middle frequency. Therefore, in order to cover the impedance of the above four parts to indicate the internal state of LIB, the starting point of the high-frequency, the semicircle vertex of the high-frequency region, the semicircle vertex of the middle-frequency region, and the starting and ending points of the low-frequency region line are directly extracted from the original data as features. The apex of the high-frequency and middle-frequency region semicircles are taken to obtain the radius of the semicircle and infer the lithium ions loss from the change of radius. In addition, more attention is paid to the middle-frequency part because the lithium ions loss part, shows small changes in the high-frequency, which means the SEI layer is relatively stable, while the middle-frequency semicircle has obvious changes. Therefore, take one point at the starting point of the high-frequency region, the vertex of the high-

frequency region semicircle, and the last point of the oblique line in the low-frequency region, and take two points for the middle frequency region semicircle. After the cyclic test, the loss of active materials and lithium inventory will inevitably occur, such as graphite spalling, electric particle cracking and the formation and decomposition of SEI film. The five points in EIS directly show degradation. In this way, the original 60 points (120 dimensions) are reduced to 5 points (10 dimensions), which not only removes low correlation data, but preserves meaningful information, simplifies the process of understanding data, and can more effectively know data changes and their significance. The fitting result of the first and last cycles, as well as the summary of R_o, R_{SEI} and R_{ct} are shown in figure S1 and table S1 respectively. In figure S1, the R_o, R_{SEI}, and R_{ct} increase after the cycle except cell 6 (figure S1 (f)). In particular, the increase in R_{ct} is the most obvious, indicating that the contact between active materials and electrolytes is deteriorating, which is related to the degradation of cells. Since the difference between cell 6 (figure S1 (f)) and the other cells, cell 6 (figure S1 (f)) is selected to be the validation in order to improve the robustness of the model. The fitted data have been given in the table S1 to show the data needed.

Figure 5 shows the selected EIS and corresponding capacity of all cells in the dataset. With the continuous test of cells, compared with the first point and the second point, the third point, the fourth point and the fifth point have more obvious upward or downward changes, which can be used to establish the aging trend of LIBs effectively. In this study, the EIS data used in the training set, validation set, and test set was generated by 4 cells at 25 ℃ and 1 cell at 35 ℃, 1 cell at 45 ℃, as well as 1 cell at 35 ℃

respectively. The detail of the dataset is shown in Figure 6. In addition, the decrease in electrochemical efficiency for all cells is shown in figure S2, which may be caused by side reactions. The test conditions of these batteries are the same except for the temperature. According to the difference in the test temperature of the battery, it can be inferred that the side reaction of the cell tested at 25 ℃ is more severe, showing an earlier electrochemical efficiency decay. The cell tested at 35 ℃ only shows after 200 cycles, while the electrochemical efficiency of the battery tested at 45 ℃ has remained stable between 99.6% and 100%.

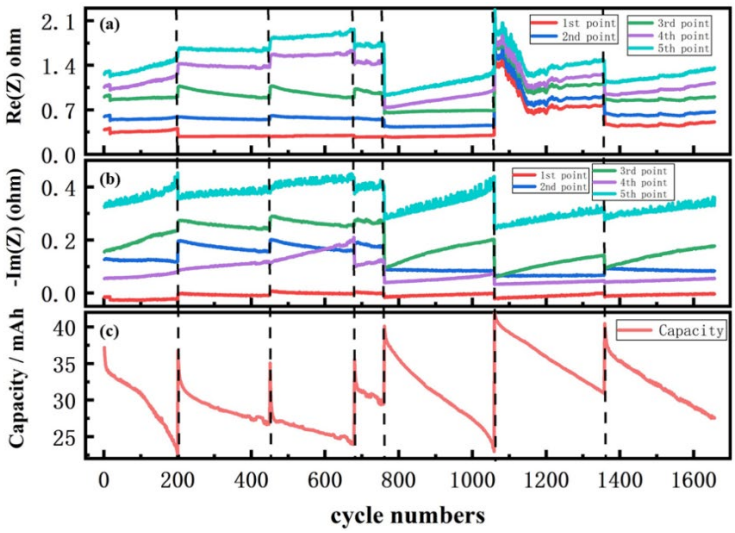

Fig. 5. Schematic diagram of changes of realia element and impractical measure in the whole life cycle of all batteries after feature extraction. (a), (b) and (c) represent the realia element of impedance, the approximate measure of impedance, and the capacity degradation respectively, and a black dotted line separates each cell. In (a) and (b), red, blue, green, purple, and cyan are respectively used to represent the selected first point, second point, third point, fourth point, and fifth point

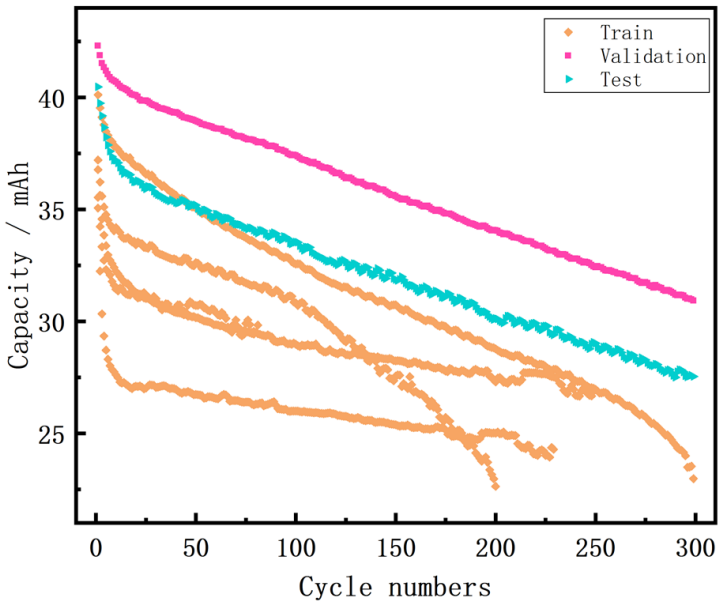

Fig. 6. Schematic diagram of dataset segmentation. Orange represents the training set, including 4 batteries tested at 25 ℃ and 1 battery at 35 ℃. Pink represents the validation set, including 1 battery tested at 45 ℃, and cyan represents the test set, including 1 battery tested at 35 ℃

2.5 Evaluation metrics

The three metrics to evaluate SOH prediction accuracy is presented in (6), (7), (8) and (9) including the root mean square error (RMSE), the mean absolute error (MAE), the mean absolute percentage error (MAPE) and the R squared (R^2).

$$RMSE = \sqrt{\frac{1}{N}\sum_{i=1}^{N}[\widehat{SOH}_i - SOH_i]^2} \quad (6)$$

$$MAE = \frac{1}{N}\sum_{i=1}^{N}|\widehat{SOH}_i - SOH_i| \quad (7)$$

$$MAPE = \frac{1}{N}\sum_{i=1}^{N}\frac{|\widehat{SOH}_i - SOH_i|}{SOH_i} \quad (8)$$

$$R^2 = 1 - \frac{\sum_{i=1}^{n}(y_i - \hat{y}_i)^2}{\sum_{i=1}^{n}(y_i - \bar{y})^2} \quad (9)$$

Where $\widehat{SOH}_i$ indicates the predicted SOH at time step i, SOH_i represents the reference value, N is the length of the SOH sequence, y_i represents the real value, $\bar{y}$ represents the average of real values, and $\hat{y}$ represents the predicted value.

3 Results

This section validates the effectiveness of the proposed feature extraction method by presenting the SOH estimation result at varied data and comparing the new approach's performance with some common baseline methodologies. The motivation of feature extraction is elaborated.

3.1 Feature extraction results

Accurately estimating the SOH of LIBs can greatly reduce the probability of accidents. The feature points and dimensions left after each feature extraction are shown in Table 1. Table 1 is divided into three parts. The method represents the code name of feature extraction, 1 represents the raw data that has not been processed, 2 represents 50% data removal on the basis of 1, in an interval manner, 3 represents 50% data removal on the basis of 2, in the same way as 2, 4 represents about 50% data removal on the basis of 2 (because 15 cannot be completely divided by 2), in the same way as before, 5 represents data removal on the basis of 4, Finally, the starting point of the high-frequency, the microscopic vertex of the high-frequency region, the microscopic vertex of the middle-frequency region, and the starting and ending points of the low-frequency region line are directly extracted from the original data as features. Points and dimensions represent the data points and data dimensions corresponding to each method. For example, point 60 in method 1 represents 60 points and 120 dimensions (including X and Y) of the original EIS curve. After feature extraction, method 5 represents the 5 most meaningful points and 10 corresponding dimensions.

Table. 1. Feature extraction method and corresponding points and dimensions corresponding to Figure 4

Method	1	2	3	4	5
Points	60	30	15	7	5
Dimensions	120	60	30	14	10

3.2 SOH estimation results at multiple data sizes

Accurately estimating the SOH of LIBs can greatly reduce the probability of accidents. In this study, we propose a simple and effective feature extraction method that effectively improves the accuracy of SOH estimation. The feature points and dimensions left after each feature extraction are shown in Table 1. As shown in Figure 7, SOH estimation results after multiple denoising are shown in the (a), (b), (c), (d), and (e) in Figure 7. It shows that the transformer-based NN can effectively capture the declining trend of the LIBs through EIS, but the estimation accuracies of methods 1 to 3 (Figures 7(a), 7(b), and 7(c)) range from -8% to 15% (shown in Figures 7(f), 7(g), and 7(h)) and are unsatisfactory. After multiple successive feature extraction, the error ranges from -4% to 5%, basically concentrated at around 1% (Figures 7 (j)). The errors overview can be seen in Table 2. Before feature extraction, the RMSE, MAE, MAPE and R^2 are 1.94, 1.67, 5.46%, and -0.055 respectively. After feature extraction, the RMSE, MAE, MAPE and R^2 of method 5 are 0.64, 0.51, 1.63% and 0.94 respectively. Especially, 80% SOH is recognized as battery retirement. In the range before 80% SOH, as shown in the green box in Figure 7 (e), the MAPE is 1.26%, while in the more

concerned range between 85% SOH and 75% SOH, as shown in the yellow box in Figure 7 (e), the MAPE is 0.67%. The results of the 95% confidence interval and distribution are shown in figure S3 to show the probability of the true value in the measurement result interval and the distribution frequency of each tiny interval. The lower limit error of the interval between method 5 and ground truth is 0.26, and the upper limit error of the interval is 0.1, while the concentration of other methods is higher, which is almost not distributed in the range below 29mAh and above 38mAh, but the confidence interval is more discrete. The experimental results show that the method is feasible and effective, and the estimation accuracy is improved through multiple feature extraction.

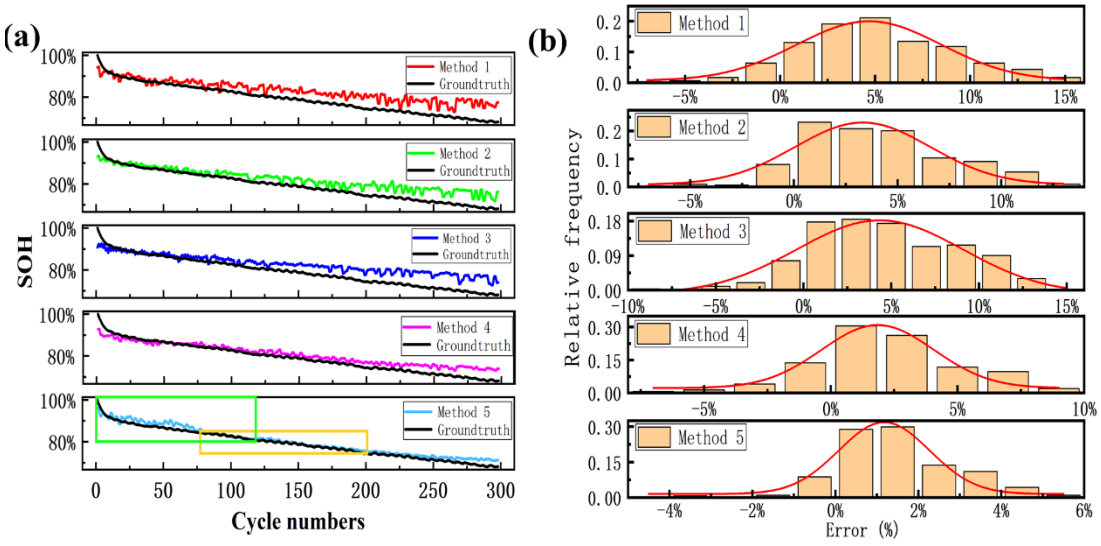

Fig. 7. SOH estimation results under different datasets using transformer-based NN. The left figure shows the SOH estimation results under different data sets. (a) Method 1 + transformer, (b) Method 2 + transformer, (c) Method 3 + transformer, (d) Method 4 + transformer, (e) Method 5 + transformer. The right-hand side figure shows the corresponding error in the left-hand side figure

Table. 2. Different SOH estimation criteria under different datasets

Metric	Method 1	Method 2	Method 3	Method 4	Method 5
RMSE	1.94	1.56	1.82	1.08	**0.64**
MAE	1.67	1.29	1.52	0.88	**0.51**
MAPE / %	5.46	4.24	5.01	3.21	**1.63**
R^2	-0.055	0.38	-0.080	0.71	**0.94**

3.3 Comparison with baseline methods

RNN-based models are used as the baseline for comparison to show that the transformer-based NN is valid. As shown in Figure 8, (a), (b), (c), and (d) show the comparison results of RNN, GRU, LSTM, and transformer-based NN using the same datasets through method 5 extraction. Results show that, the transformer-based NN effectively learned the nonlinear attenuation process in the early stage of SOH, and maintained 98.73% estimation accuracy before 80% SOH of the rated value, while the estimation results of the other three models are unsatisfactory. The specific errors are presented in Table 3. The best RMSE, MAE, MAPE and R^2 of the three models (RNN, GRU, LSTM) are 1.17, 1.14, 3.62% and 0.80 respectively, 45%, 55%, 55% and 17% respectively worse than those using the transformer-based NN. We speculate that the EIS data has abundant and high dimensions information, so the hidden relationship can be learned more effectively through the self-attention in the transformer, hence achieving better estimation accuracy.

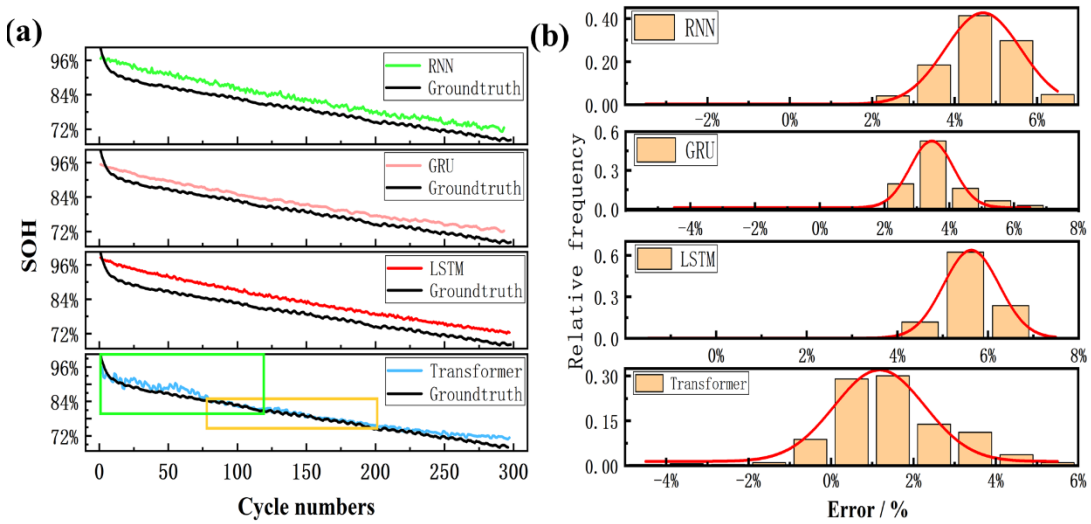

Fig. 8. SOH estimation results under different models. The left figure shows the SOH estimation results under different data sets. (a) Method 5 + RNN, (b) Method 5 + GRU, (c) Method 5 + LSTM, (d) Method 5 + transformer. The right figure shows corresponding error in the left figure

Table. 3. Different SOH estimation criteria under different models

Metric	RNN	GRU	LSTM	transformer
RMSE	1.51	1.17	1.80	**0.64**
MAE	1.46	1.14	1.77	**0.51**
MAPE / %	4.57	3.62	5.57	**1.63**
R^2	0.73	0.80	0.61	**0.94**

4 Conclusions

In this paper, we propose a method for estimating the SOH of LIBs by extracting the feature points of EIS and using transformer-based NN. EIS data has the advantage of utilizing the rich information contained in EIS such as material properties and electrochemical reactions, which is supported by relevant mechanisms, for SOH

estimation. Through feature extraction, features with low correlation with capacity degradation are removed and the SOH estimation accuracy is effectively improved. Based on the high dimensionality of EIS data, we used the transformer-based NN as the estimation model, which can capture the abundant information hidden in the data. The baseline comparison results show that, when using high-dimensional data such as EIS, the transform NN model can capture more information and achieve better estimation performance. RMSE, MAE, and MAPE were used in the error evaluation, which was 0.64, 0.51, and 1.63% respectively in the whole cycle life. The evaluation metrics prove the effectiveness of the proposed method. These findings may be used in the routine inspection of LIB in the future, to improve safety.

Acknowledgement

We gratefully acknowledge the financial support from the National Key Research and Development Program of China (2022YFE0202400).

References

[1] D. Bresser, K. Hosoi, D. Howell, H. Li, H. Zeisel, K. Amine, S. Passerini, Perspectives of automotive battery R&D in China, Germany, Japan, and the USA, J. Power Sources. 382 (2018) 176-178. https://doi.org/10.1016/j.jpowsour.2018.02.039.

[2] G. Harper, R. Sommerville, E. Kendrick, L. Driscoll, P. Slater, R. Stolkin, A. Walton, P. Christensen, O. Heidrich, S. Lambert, A. Abbott, K. Ryder, L. Gaines, P. Anderson, Recycling lithium-ion batteries from electric vehicles, Nature. 575 (2019) 75-86. https://doi.org/10.1038/s41586-019-1682-5.

[3] E. Wood, M. Alexander, T. H. Bradley, Investigation of battery end-of-life conditions for plug-in hybrid electric vehicles, J. Power Sources. 196 (2011) 5147-5154. https://doi.org/10.1016/j.jpowsour.2011.02.025.

[4] X. Hu, L. Xu, X. Lin, M. Pecht, Battery Lifetime Prognostics, Joule. 4 (2020) 310-346. https://doi.org/10.1016/j.joule.2019.11.018.

[5] R. N. Methekar, P. W. C. Northrop, K. Chen, R. D. Braatz, V. R. Subramanian, Kinetic Monte Carlo Simulation of Surface Heterogeneity in Graphite Anodes for Lithium-Ion Batteries: Passive Layer Formation, J. Electrochem. Soc. 158 (2011) A363. https://doi.org/10.1149/1.3548526.

[6] A. Guha; A. Patra; K. V. Vaisakh, Remaining useful life estimation of lithium-ion batteries based on the internal resistance growth model, 2017 Indian Control Conference (ICC). (2017) 33-38. https://doi.org/10.1109/INDIANCC.2017.7846448.

[7] B. Saha, S. Poll, K. Goebel, J. Christophersen, An integrated approach to battery health monitoring using bayesian regression and state estimation, 2007 IEEE Autotestcon. (2007) 646-653. https://doi.org/10.1109/AUTEST.2007.4374280.

[8] V. Ramadesigan, K. Chen, N. A. Burns, V. Boovaragavan, R. D. Braatz, V. R. Subramanian, Parameter Estimation and Capacity Fade Analysis of Lithium-Ion Batteries Using Reformulated Models, J. Electrochem. Soc. 158 (2011) A1048. https://doi.org/10.1149/1.3609926.

[9] Y. Liu, X. Zou, Z. Yang, S. Shi, Machine Learning Embedded with Materials Domain Knowledge, J. Chin. Ceram. Soc. 50 (2022) 863-876. https://doi.org/10.14062/j.issn.0454-5648.20220093.

[10] M. Berecibar, F. Devriendt, M. Dubarry, I. Villarreal, N. Omar, W. Verbeke, J. V. Mierlo, Online state of health estimation on NMC cells based on predictive analytics, J. Power Sources. 320 (2016) 239-250. https://doi.org/10.1016/j.jpowsour.2016.04.109.

[11] K. Luo, X. Chen, H. Zheng, Z. Shi, A review of deep learning approach to predicting the state of health and state of charge of lithium-ion batteries, J. Energy Chem. 74 (2022) 159-173. https://doi.org/10.1016/j.jechem.2022.06.049.

[12] P. Khumprom, N. Yodo, A Data-Driven Predictive Prognostic Model for Lithium-ion Batteries based on a Deep Learning Algorithm, Energies. 12 (2019) 660. https://doi.org/10.3390/en12040660.

[13] L. Song, K. Zhang, T. Liang, X. Han, Y. Zhang, Intelligent state of health estimation for lithium-ion battery pack based on big data analysis, J. Energy Storage. 32 (2020) 101836. https://doi.org/10.1016/j.est.2020.101836.

[14] D. Roman, S. Saxena, V. Robu, M. Pecht, D. Flynn, Machine learning pipeline for battery state-of-health estimation, Nat. Mach. Intell. 3 (2021) 447-456. https://doi.org/10.1038/s42256-021-00312-3.

[15] N. Yang, Z. Song, H. Hofmann, J. Sun, Robust State of Health estimation of lithium-ion batteries using convolutional neural network and random forest, J. Energy Storage. 48 (2022) 103857. https://doi.org/10.1016/j.est.2021.103857.

[16] S. Shen, M. Sadoughi, X. Chen, M. Hong, C. Hu, A deep learning method for online capacity estimation of lithium-ion batteries, J. Energy Storage. 25 (2019) 100817. https://doi.org/10.1016/j.est.2019.100817.

[17] S. Hochreiter, J. Schmidhuber, Long Short-Term Memory, Neural Computation. 9

(1997) 1735-1780. https://doi.org/10.1162/neco.1997.9.8.1735.

[18] K. Cho, B. v. Merriënboer, C. Gulcehre, D. Bahdanau, F. Bougares, H. Schwenk, Y. Bengio, Learning Phrase Representations using RNN Encoder–Decoder for Statistical Machine Translation, Association for Computational Linguistics. (2014) 1724-1734. https://doi.org/10.3115/v1/D14-1179.

[19] A. Eddahech, O. Briat, N. Bertrand, J.-Y. Delétage, J.-M. Vinassa, Behavior and state-of-health monitoring of Li-ion batteries using impedance spectroscopy and recurrent neural networks, Int. J. Elec. Power. 42 (2012) 487-494. https://doi.org/10.1016/j.ijepes.2012.04.050.

[20] F. Heinrich, M. Pruckner, Virtual experiments for battery state of health estimation based on neural networks and in-vehicle data, J. Energy Storage. 48 (2022) 103856. https://doi.org/10.1016/j.est.2021.103856.

[21] Z. Chen, H. Zhao, Y. Zhang, S. Shen, J. Shen, Y. Liu, State of health estimation for lithium-ion batteries based on temperature prediction and gated recurrent unit neural network, J. Power Sources. 521 (2022) 230892. https://doi.org/10.1016/j.jpowsour.2021.230892.

[22] S. Cui, I. Joe, A Dynamic Spatial-Temporal Attention-Based GRU Model With Healthy Features for State-of-Health Estimation of Lithium-Ion Batteries, IEEE Access. 9 (2021) 27374-27388. https://doi.org/10.1109/ACCESS.2021.3058018.

[23] K. A. Severson, P. M. Attia, N. Jin, N. Perkins, B. Jiang, Z. Yang, M. H. Chen, M. Aykol, P. K. Herring, D. Fraggedakis, M. Z. Bazant, S. J. Harris, W. C. Chueh, R. D. Braatz, Data-driven prediction of battery cycle life before capacity degradation, Nat.

Energy. 4 (2019) 383-391. https://doi.org/10.1038/s41560-019-0356-8.

[24] K.-H. Tseng, J.-W. Liang, W. Chang, S.-C. Huang, Regression Models Using Fully Discharged Voltage and Internal Resistance for State of Health Estimation of Lithium-Ion Batteries, Energies. 8 (2015) 2889-2907. https://doi.org/10.3390/en8042889.

[25] Z. Lin, M. Feng, C. N. d. Santos, M. Yu, B. Xiang, B. Zhou, Y. Bengio, A Structured Self-attentive Sentence Embedding, ICLR. (2017) arXiv: 1703.03130.

[26] A. Dosovitskiy, L. Beyer, A. Kolesnikov, D. Weissenborn, X. Zhai, T. Unterthiner, M. Dehghani, M. Minderer, G. Heigold, S. Gelly, J. Uszkoreit, N. Houlsby, An Image is Worth 16x16 Words: Transformers for Image Recognition at Scale, ICLR. (2020) arXiv: 2010.11929.

[27] J. Cheng, L. Dong, M. Lapata, Long Short-Term Memory-Networks for Machine Reading, Proceedings of the 2016 Conference on Empirical Methods in Natural Language Processing. (2016) arXiv: 1601.06733.

[28] L. Wu, X. Liu, Q. Liu, Centroid Transformers: Learning to Abstract with Attention, arXiv. (2021) arXiv: 2102.08606.

[29] A. Vaswani, N. Shazeer, N. Parmar, J. Uszkoreit, L. Jones, A. N. Gomez, L. Kaiser, I. Polosukhin, Attention Is All You Need, Advances in neural information processing systems. 30 (2017) arXiv: 1706.03762.

[30] M. Gaberšček, Understanding Li-based battery materials via electrochemical impedance spectroscopy, Nat. Commun. 12 (2021) 6513. https://doi.org/10.1038/s41467-021-26894-5.

[31] D. Bahdanau, K. Cho, Y. Bengio, Neural Machine Translation by Jointly Learning

to Align and Translate, (2014) arXiv: 1409.0473.

[32] Y. Zhang, Q. Tang, Y. Zhang, J. Wang, Stimming, U. and Lee, A. A., Identifying degradation patterns of lithium ion batteries from impedance spectroscopy using machine learning, Nat. Commun. 2020. https://doi.org/10.5281/zenodo.3633835.

[33] K. Lin, S. Yang, Z. Shi, Q. Fan, Z. Liu, L. Liu, Knitting a sweater with UV-induced in situ polymerization of poly (pyrrole-co-citral nitrile) on Ni-rich layer oxide cathode materials for lithium ion batteries, J. Power Sources. 520 (2022) 230768. https://doi.org/10.1016/j.jpowsour.2021.230768